# Optical Biometry

10

Magdalena Nenning, Nino Hirnschall, and Oliver Findl

Cataract surgery has greatly improved by innovative techniques and advanced technology. Patients' expectations and demands for an optimal outcome have increased and have contributed to the fact that, besides obtaining visual rehabilitation, it has also become a refractive procedure.

An accurate calculation of intraocular lens (IOL) power is crucial for satisfactory refractive outcomes. Several factors, including keratometry (K) readings, axial length (AL), postoperative IOL position, and IOL power formulae, affect the IOL power calculation, with preoperative biometry, primarily the assessment of the axial eye length, being its most essential component. Postoperative refractive errors are the main cause for dissatisfaction or lens exchange, and studies have shown that 54% of those errors arise from imprecise AL measurements. Historically, measurements of AL, ACD, and crystalline lens thickness have been commonly performed by ultrasound biometry.

The introduction of optical biometry was a major development in cataract surgery and has led to more precise biometry systems that are now considered as the gold standard in ocular biometry [1–3].

## History of Optical Biometry

### Ultrasound Biometry

Since its introduction in 1956, ultrasound biometry has steadily improved and has been the gold standard for AL measurement before the introduction of partial coherence interferometry [2, 4]. Two types of A-scan ultrasound biometry are available.

In contact applanation biometry, an ultrasound probe is directly placed on the central cornea and a high frequency sound wave travels into the eye, with part of it reflecting back toward the probe when encountering a media interface, allowing to calculate the distance between the probe and various intraocular structures. A limitation to this method is the inadvertent indentation of the cornea and the resulting shallowing of the anterior chamber which arises from the compression of the probe. This results in a shortening of the eye and an overestimation of the IOL power. Since

M. Nenning · O. Findl (✉)
Vienna Institute for Research in Ocular Surgery (VIROS), A Karl Landsteiner Institute, Hanusch Hospital, Vienna, Austria
e-mail: oliver@findl.at

N. Hirnschall
Department for Ophthalmology and Optometry, Kepler University Hospital GmbH, Linz, Austria
e-mail: nino@hirnschall.at


J. Aramberri et al. (eds.), *Intraocular Lens Calculations*, Essentials in Ophthalmology,
https://doi.org/10.1007/978-3-031-50666-6_10

this error is variable, it cannot be compensated for by a constant.

In immersion ultrasound biometry, a saline immersion bath is placed between the probe and the eye. While avoiding the indentation of the cornea, this method was shown to be more accurate compared to contact ultrasound. A mean difference of 0.25–0.33 mm has been reported between the two methods, which translates to an error of approximately 1 diopter (D) [1, 5, 6].

In A-scan ultrasound biometry in general, relatively long, low-resolution wavelengths (10 MHz) are used. This has the advantage of excellent penetration through dense media, but the disadvantage of low resolution. An accuracy of AL measurement of approximately 100–200 µm has been reported, whereas an error of 100 µm results in a corresponding postoperative refractive error of 0.28 D. Also, inconsistent measurements may occur due to discrepancies of retinal thickness in the central retina and off-axis measurements [1, 5, 6].

## Partial Coherence Interferometry (PCI)

Although the birthplace of optical biometry is Vienna, Austria, the concept of coherence interferometry was introduced before as a new method for high-range resolution measurement of light scattering in optically dense inhomogeneous media in the 1970s [7].

However, it was not until 1986, when Fercher and coworkers introduced this method for the purpose of ocular biometry [8]. They used a long-coherence Helium-Neon laser beam to illuminate the patient's eye, which represented an interferometer with the cornea and the retina forming the interferometer mirrors. The reflections from the cornea and the retina created an interferogram consisting of concentric interference fringes (Fig. 10.1), which pulsated with the patient's heartbeat. An interferometer in the illuminating beam enabled the determination of the optical path length between those two mirrors. This technique offered the advantages of high transversal resolution at the fundus and no need for anesthesia or mechanical contact with the eye [9].

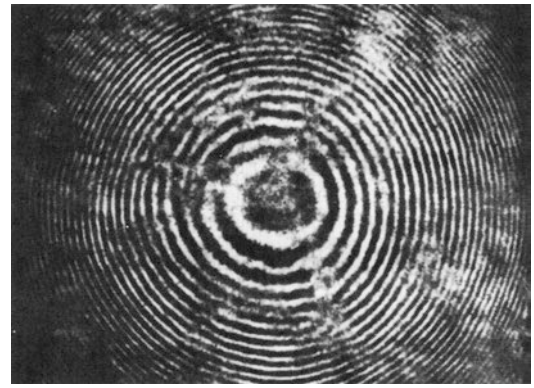

**Fig. 10.1** Interference pattern caused by the light remitted by the fundus and the light reflected at the cornea [9]

The use of a low temporal coherence allowed accurate measurement of intraocular distances, especially the axial eye length. On the contrary, high temporal coherence was used to measure distance variations resulting from blood pulse-induced dilatation of ocular tissues, which contributed to clinical applications in vascular diseases or glaucoma [8].

Concerning the axial eye length measurement, however, it was difficult to meet the requirements such as a high spatial coherence and a very low temporal coherence in those early times. Until 1985, dye lasers, which suffered from problems like beam instabilities, were used and later replaced with multimode semiconductor lasers, which, on the other hand, offered only low spectral bandwidth [8].

In early experiments with a Michelson interferometer, an optical dual-beam illumination scheme was used. A short coherence length beam was split into a direct and a delayed beam, and the eye was illuminated along a coaxial pathway. An overlapping of the two exit beams, reflected at fundus and cornea, indicated an identical total path length, and an interferogram was created at the observation plane.

Figure 10.2 shows an A-scan of a myopic eye, measured by PCI as described above. The peak position indicates the optical distance to the anterior corneal surface, which, in this case, yields an

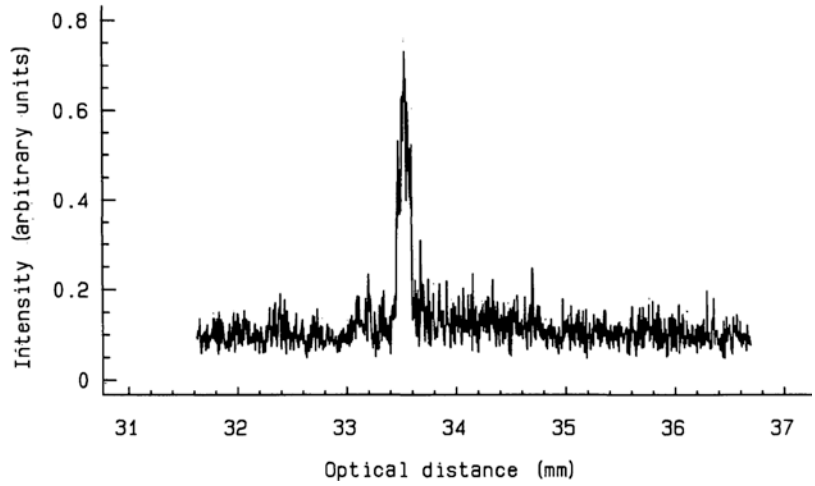


**Fig. 10.2** A-scan of a myopic eye, measured with the first dual-beam heterodyne PCI instrument. The signal peak indicates the optical length of the eye (33.56 mm). Divided by the refractive index of the ocular media in sum, the geometrical length of the eye can be obtained (24.78 mm) [10]

optical length of 33.56 mm. This value has to be divided by the group refractive index of the traversed ocular media to convert to a geometric length of 24.78 mm [10]. Later, the resolution was further refined by replacing the multimode laser diode by a broadband superluminescent diode, which allowed measurements of the cornea and anterior segment [8].

In the meantime, the PCI method has almost completely replaced ultrasound-based biometry.

Its commercial launch took place in 1999 by Zeiss with the introduction of the IOL Master (Carl Zeiss Meditec AG, Germany), while several other devices of various manufacturers have been developed later (Lenstar LS900, Haag-Streit; Aladdin, Topcon; OA-2000, Tomey; AL-Scan, Nidek; Galilei G6, Ziemer, etc.). All optical biometry devices are somewhat based on the concept of PCI [11].

## Ultrasound Biometry vs. PCI

A direct comparison between ultrasound and optical biometry cannot be drawn, as ultrasound biometry measures the distance from the cornea to the inner limiting membrane, while optical biometry measures the distance from the cornea to the retinal pigment epithelium, which explains a discrepancy in axial length values obtained from these two methods. Therefore, the optical biometry measurements were "adjusted" to be interchangeable with immersion ultrasound measurements (with a correction factor of 0.18 mm) [5].

Optical biometry is superior to ultrasound biometry in several aspects. Orientation is easier for optical biometry because the patient fixates the laser beam, whereas orientation of the scan is more of an estimation for ultrasound measurements. Other advantages of optical biometry are that it is examiner independent, easy to be performed, and there is no risk of infection [5].

Regarding the prediction of IOL power, it was shown that PCI can improve the refractive outcome by about 30% when using the SRK II formula [1]. In a study that compared PCI with ultrasound biometry by applying both methods to four commonly used IOL power formulae (SRK II, Olsen, SRK/T, Holladay I), the refractive outcome was significantly improved with all four IOL power formulae when using PCI instead of ultrasound [12].

One limitation of optical biometry is the absorption and reflection of light in dense media resulting in unsuccessful scans in the case of very dense cataracts or corneal scars.

Optical biometry has replaced ultrasound biometry worldwide, with an exception in cases of very dense cataracts [13].

## Concept of PCI

Figure 10.3 shows a diagram of the principal setup of a dual-beam partial coherence interferometer. A superluminescent diode (SLD) emits an infrared light beam ($\lambda \sim 780$ nm) of high spatial coherence but very short coherence length ($l_c$). Long, red wavelengths are chosen because they are scattered less than blue light. This results in a better penetration in dense cataracts. The SLD emits a broader spectrum of color than does a laser, so the measurement is more sensitive than it would be with only one frequency of light. An external Michelson interferometer splits the beam into two parts by means of a fixed reference mirror (1) and a moveable measurement mirror (2), resulting in a reference beam and a measurement beam. Those two beam components are parallel and coaxial and due to being reflected once at both interferometer plates, they have a mutual time delay of twice the interferometer arm length difference ($d$). At the interferometer exit, they are combined again, forming a coaxial dual beam [1, 10, 14, 15, p. 261]

The laser beam appears as a weak red spot (the wavelength is just visible), which acts as a fixation target for the patient [16]. The eye is illuminated, and reflected beams are generated at every intraocular interface, splitting both beam components into further subcomponents. Hence, two coaxial beams that are both reflected at the cornea ($C$) and the retina ($R$) result in four reflected beams, yielding an additional path difference of twice the optical length (OL) between each of the two pairs of beams [10]. The total of the reflected beams is detected by and superimposed on a photodetector.

The axial eye length, in this method, extends from the anterior corneal surface to the retinal pigment epithelium, so the reflections of those two interfaces are measured. If the coherence length of the laser is shorter than two times the optical length, no interference will be observed. If, however, the delay of these two beam components produced by the interferometer (the interferometer arm length difference) equals the optical distance between the two interfaces, there are two subcomponents that traverse the same total path length and will consequently interfere. That means, two arm length differences equal twice the optical length within a difference of the coherence length. For AL measurement, the subcomponent of the reference beam that is reflected at the retinal pigment epithelium ($R_1$) will interfere with the subcomponent of the measurement beam that is reflected at the cornea ($C_2$) [14]. The photodetector senses the intensity distribution (the interference pattern consists of concentric fringes) and records the corresponding displacement of the measurement mirror and the interferometer arm length difference, respectively. As the mirror position can be determined precisely, this method yields very accurate results [17, p. 129].

Each interferometer arm length difference for which an interference pattern is observed equals an intraocular optical distance within the coherence length of the light source. The interference pattern is called a partial coherence interferometry signal, similar to that of ultrasound A-scans, but with a much higher resolution (approximately 12 m) and precision (0.3–10 m). The anterior corneal surface acts as the reference surface, for all intraocular distances are measured from this point. Hence, any influence of longitudinal eye movement during measurement can be neglected [1, 14].

In order to accelerate the process, a dynamic approach based on the heterodyne detection principle has been established. In this technique, the measurement mirror is shifted with constant speed by a stepper motor. This causes a Doppler shift of the light frequency of the measurement beam, where

$$f_D = 2v / \lambda$$

$v$ is the speed with which the mirror is moved (plate speed), and $\lambda$ is the wavelength of light.

Interference patterns will occur in case of path length coincidence, as described above, but in this case, intensity is modulated by the Doppler frequency. A photodetector measures and amplifies the intensity of the reflected beams and a band pass filter is interposed, which digitally filters the signals in a manner that it only transmits signals with the Doppler frequency $f_D$. A personal

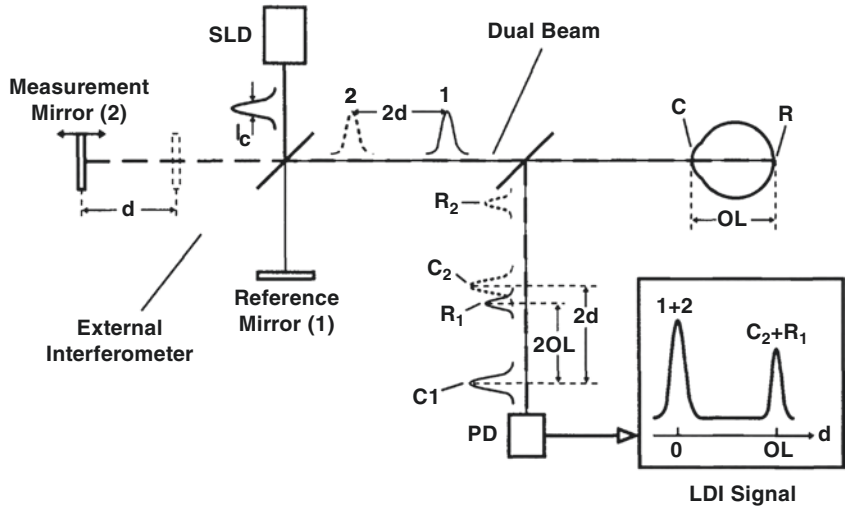


**Fig. 10.3** Principle of the dual-beam PCI. An external Michelson interferometer illuminates the eye with a coaxial dual beam. The reflections are detected by and superimposed on a photodetector. A partial coherence interferometry signal of the optical distance is imaged, which equals the optical axial eye length [14]

computer records the intensity of the measured signal as a function of $d$ and displays it as an LDI scan as shown in Fig. 10.3. At $d = 0$, the two beam components (1 + 2) interfere, which is shown as a peak in the scan that can be considered as a calibration point. At $d$ = OL, the two beam components $R_1$ and $C_2$ interfere and the resulting peak corresponds with the optical distance between $C$ and $R$ [10, 14].

Calibration of the instrument can be performed by measuring the optical length of a plane glass pate of known thickness and refractive index. Once the instrument is calibrated, $d$ doesn't have to be measured along the total eye length, but instead, $d$ = OL is located and a surrounding range of up to 3 mm is scanned to register the field in which retinal peaks are expected. The LDI scans therefore only contain the peak at $d$ = OL, whereas the peak at $d = 0$ is waived. The information gathered this way suffices to measure the AL and the retinal thickness and helps to decrease the measuring time as well as the computer storage space needed [10, 14].

.An additional helium neon (HeNe) laser and a single-mode laser diode (SMLD) serve for alignment purposes. The latter has the same wavelength as the measurement beam, but an $l_c$ larger than twice the OL. Hence, regardless the interferometer arm length difference, permanent interference happens for the reflected beams and since $\lambda$ is the same, no difference is visible in the interference pattern. This procedure helps to align the photodetector with the center of the interference fringes before starting the measurement. Once finished, the laser input can simply be switched from SMLD to SLD [10].

The coherence length of the light source correlates directly with the precision of the measurement: the shorter the $l_c$, the higher the accuracy. A signal with $f_D$ is usually recorded in the range $d$ = OL ± $l_c/2$, while the amplitude of the signal varies within this range and its maximum is obtained at $d$ = OL. Therefore, if the signal peak is located, the precision is higher than $l_c/2$. Hence, an SLD that emits a light beam with an $l_c$ of 15 µm achieves a precision <7.5 µm [10, 14].

Since the concept of dual-beam PCI is to match an unknown intraocular distance with a known distance within the Michelson interferometer and the cornea is used as a reference surface, the location of the eye relative to the instrument is insignificant for the measurement and longitudinal eye movement doesn't impair the procedure. Lateral eye movements, on the other hand, are capable of influencing the measurement [14].

PCI yields optical distances, so the values obtained need to be divided by the group refractive index of the traversed ocular media (cornea, aqueous humor, lens, vitreous) to convert to geometrical distances [1].

The IOL Master uses PCI for AL measurement, while the ACD is measured by optical principles using not a PCI method but rather a photographic technique. The first commercially available PCI instrument for anterior segment biometry was the AC Master (Carl Zeiss Meditec AG). Measurements of the anterior segment using PCI have to be performed along the optical axis, so the device includes a display to steer the direction of fixation of the eye. This mechanism also enables to present a defocus in order to induce accommodation; thus, the AC Master can also be used during accommodation [18, 19]. The technique of PCI for anterior segment biometry measures central corneal thickness, ACD, and lens thickness with high precision and reproducibility [20, 21].

The PCI technique as described above has been extended to a fully computerized scanning instrument. It is not only capable of measuring intraocular distances parallel to the visual axis but also at arbitrary angles. The performance of scans in horizontal and vertical directions facilitates to maintain topographic and tomographic images as well as cross-sectional images and thickness maps of different fundus structures [14].

As measurements are carried out in vivo, the laser safety regulations have to be met. The intensity of about 190 μW (or 490 μW/cm$^2$) of the SLD is allowed to be applied to the eye for approximately 47 min. Maximum illumination time of one point of the eye in this procedure is about 2–4 s, which is far below the safety limit. The HeNe alignment laser delivers a power of approximately 5 μW (or 13 μW/cm$^2$), which is below the limit of permanent illumination of 18 μW/cm$^2$ [14].

## Optical Low-Coherence Reflectometry (OLCR)

Related to PCI technology, OLCR was introduced in the form of Lenstar LS900 (Haag-Streit AG, Switzerland), followed by the Aladdin (Topcon, Japan). Those devices use a laser diode infrared light with a wavelength of 820 nm. Similar to PCI, the concept is based on a Michelson interferometer and an A-scan is obtained as a result. While the devices differ in AL measurement, the same technology is used to measure keratometry readings and corneal diameter distance. OLCR-based devices are capable of acquiring central corneal thickness and lens thickness, and all measurements are obtained simultaneously, without the need for realignment. The difference of the results from both methods has found to be clinically irrelevant [22–24].

## Advancements of PCI

Although optical biometry is preferred over ultrasound biometry due to higher accuracy and comfort of the method, one relevant drawback of this technique is its inability to be performed in cases with dense opacities of the cornea or the lens [25].

The accuracy of PCI is strongly related to the signal-to-noise ratio (SNR), which is the ratio of the interference signal amplitude relative to the background noise amplitude. A high SNR reflects higher quality of the AL readings and for a measurement to be reliable, a ratio above 2.0 has been determined. Values between 1.6 and 1.9 are classified as borderline and should entail additional measurements for verification [26, 27].

Main reason for a low SNR and the failure to perform a PCI measurement is the presence of very dense media, such as dense corneal scars, dense cataracts, or a vitreous hemorrhage. Other reasons include patients with poor fixation and macular pathologies [25]. These opacities are capable of causing different optical phenomena, such as absorption, reflection, and light scattering (particularly Rayleigh scattering). Any opacity in media traversed by the laser can interfere with the result, but above all, mature cataracts and particularly posterior subcapsular cataracts were responsible for the first generations of PCI measurement failures. In such cases, the SNR may amount to less than 2.0, which requires ultrasound biometry to be performed subsequently in order to gain AL readings [25].

To overcome this problem, software and hardware upgrades of the commonly used biometers have been developed [24]. In the first approach, the averaging of consecutive scans was used to increase the SNR by dampening all noise variance, including shot noise. As a result of this method, structural elements, that have been hidden under the noise floor, became visible. However, one remaining problem was that actual signals were low in amplitude [28].

In the second approach to enhance image quality, the so-called composite scan was introduced in a software upgrade (version 5.0) of the IOL Master 500. The composite scan allows averaging of consecutive optical scans by digital processing of signals of multiple measurements. As true peaks, although low in amplitude, are present in multiple scans, their signal enhances as more scans are performed. Background noise, on the other hand, is a random signal, so by superimposing multiple scans, those peaks cancel each other out. This technique helps to improve the SNR and therefore allows to successfully gain biometry readings in part of the eyes that previously failed the measurement. A clinical evaluation of the composite scan showed that the rate of acquisition failure could be reduced from 10.6% to 4.7%. The new algorithm was successful in 30% of the eyes that could not be measured with version 4.0 of the IOL Master 500 and was particularly advantageous in eyes with posterior subcapsular cataract [25].

## Introduction of OCT-Based Biometry

In 1991, Huang and coworkers adapted the technique of low-coherence reflectometry with the aim of generating not only one-dimensional (A-Scan), but two-dimensional (B-Scan) images of biological tissues. Although its predecessor and basic ranging technology was applied since the 1970s, as mentioned earlier in this chapter, it was with this development that the term optical coherence tomography was first introduced [1, 8, 29].

The process of creating a one-dimensional, longitudinal scan is repeated at incremental steps across the tissue sample, and the reflection sites in those individual scans are brought together to provide a two-dimensional map [30].

The operating mode is therefore analogous to ultrasonic pulse-echo imaging (ultrasound B-mode), and the device utilized is an extension to previously used low-coherence reflectometers. An incorporated transverse scanning mechanism enables two-dimensional imaging, and higher-speed longitudinal scanning increases the data collection rate. The amplitudes and delays of tissue reflections are measured similarly to the PCI method, and the lateral resolution of the image is limited by the beam diameter. The resulting image can be viewed directly as a gray scale or false-color image. The optical sectioning capability of OCT is similar to confocal microscopic systems. However, it bears the advantage of not being limited by the available numerical aperture but only by the coherence length of the light source. Thus, high-resolution, transpupillary imaging of the posterior eye can be achieved [29].

The change from A-scan to B-scan was a major development in ophthalmic imaging. By generating cross-sectional slices of tissue, peaks can directly be assigned to their corresponding tissue structures and boundaries can be verified, which prevents from potential errors. Furthermore, OCT-based biometry is able to image a longitudinal cross section through the entire length of the eye including the anterior segment, which makes it a useful imaging tool particularly in irregular cataracts or eyes with phakic IOLs, but also in pseudophakic eyes in order to measure postoperative ACD.

A direct comparison between an A-scan from the IOL Master 500 (Fig. 10.4) and a B-scan from the IOL Master 700 (Fig. 10.5) demonstrates that the added information B-scans provide on ocular tissues.

### Time-Domain OCT

Traditional OCT imaging, as introduced in 1991, uses time-domain detection. A low-coherence light source is coupled into the interferometer

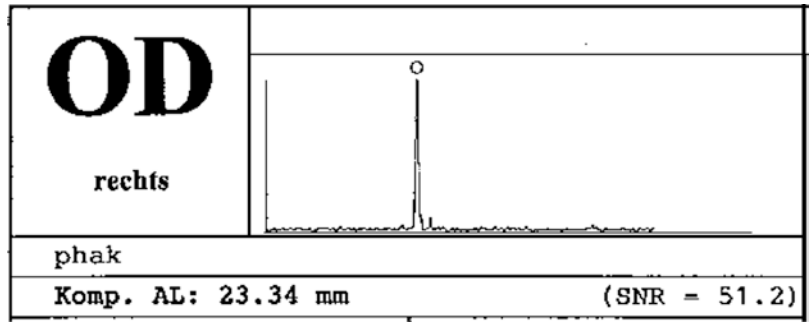


**Fig. 10.4** A-scan (IOL Master 500)

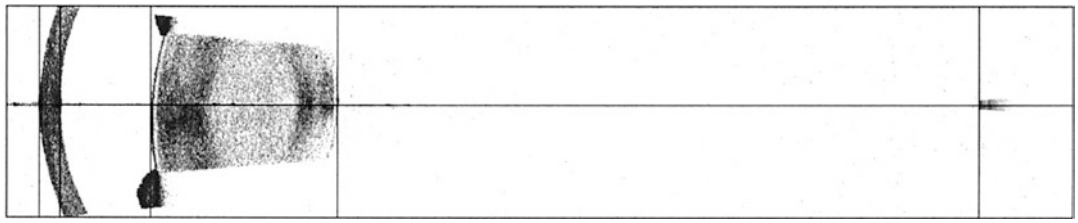

**Fig. 10.5** B-scan (IOL Master 700)

and split into two components by a beam splitter. One arm of the interferometer aims a beam to the sample being investigated while the other arm directs a beam to a reference mirror. The signals from both arms are then reflected and scattered back and recombined by the beam splitter, which lies in the path from the light source to the sample, before being sensed by a photodetector [30].

In time-domain OCT (TD-OCT), the position of the reference mirror is displaced by a stepper motor. The photodetector detects interferometric signals only when the reflections from both interferometer arms are nearly matched in group delay (time-of-flight) and the amplitude of the interferometric signal is highest, when the reference arm length is matched to the backscattering interface's distance, or, in other words, when the two arms are matched in distance so that the reflections reach the detector at the same time [29]. The photodetector records the amplitude of the signal and simultaneously, the corresponding position of the reference mirror is scanned in order to measure amplitudes and delays of tissue reflections. Usually, a piezoelectric transducer in the sample arm is used to measure the length of the optical delay line. The detector output generates the interferometric signals, which are collected by a computer and, after sophisticated processing, produce a cross-sectional image. Multiple of those parallel images can be used to gather a three-dimensional data set.

The broadness of the interference signal is given by the coherence length; the short coherence length and broad spectral bandwidth of the light source cause the signal to fall off rapidly with delay mismatch and by observing the interference peaks during the scan, the location of the reflections from the sample can be determined with high resolution [29–31, p. 12ff].

Eye motion during measurement is capable of decreasing the resolution and the SNR in OCT imaging. In TD-OCT, movement only affects the image pixel for which the signal is captured at that time, so those artefacts are usually insignificant. TD-OCT B-scans have an axial resolution of approximately 10 µm and a transverse resolution of 20–25 µm. To increase the resolution and scan density, the scan time can be prolonged in order to achieve more A-scans that contribute to the final image. However, as the scan time increases, so does the likelihood of eye motion-induced artefacts [30, 32].

## Spectral-Domain OCT

In 2006, the first Spectral-Domain OCT (SD-OCT) device became available on the market. The principle of SD-OCT, also known as Fourier-Domain OCT (FD-OCT) or Frequency-Domain OCT, is similar to that of TD-OCT. However, instead of changing and scanning the position of the reference mirror, it is fixed and stationary at one position; hence, no mechanical scanning of its location is required. The interference pattern is recorded as a function of optical frequency with a spectrometer, instead of a photodetector and Fourier transformation is applied to convert the interferogram to a frequency-domain spectrum [33]. The spectrometer is a charge-coupled device (CCD) with an array of photodetectors that are each sensitive to a certain range of frequencies. The CCD senses all frequency components of the interference pattern, and all components of the spectral variation of the detected signal correspond to a specific depth within the tissue. Fringe patterns from closer tissue planes are spaced farther apart than those arising from deep tissue interfaces, and higher reflective tissues result in higher amplitude interferograms. Thus, the information needed to produce an A-scan is obtained from the spacing and amplitude of the fringe pattern. Similar to TD-OCT, multiple A-scans are acquired along a transverse plane and assembled into B-scans [15, p. 261, 30, 32, 33].

SD-OCT is principally more prone to motion-induced signal fading, since the signal is detected over time from various interfaces of different depths inside the tissue, but as imaging speed is easy to increase in SD-OCT systems, those motion artefacts can be reduced to a minimum. A lower illumination time achieved by a pulse instead of a broadband light source further helps to alleviate this problem. Moreover, motion-induced artefacts can be compensated for by image registration, which is a technique that aligns multiple B-scans based on structural features of the tissue examined, such as blood vessels [30, 32].

The introduction of FD-OCT not only depicted the foundation of all modern OCT systems today but also for functional extensions such as OCT angiography [8].

## Swept-Source SD-OCT

The swept-source version of SD-OCT became available in clinical practice in 2012, with the IOL Master 700 (Carl Zeiss Meditec AG) being the first Swept-Source OCT (SS-OCT)-based biometry device.

SS-OCT is a variation of FD-OCT, in which a Fourier transformation is applied to the interference pattern to convert measurements of interfered light into physical delays or distances to allow simultaneous measurements of all light echoes.

In SS-OCT, the SLD's band of frequencies is replaced with a rapidly tunable narrowband laser. Instead of separating the broad wavelength light into single wavelength components by a spectrometer, the tunable swept laser emits different wavelengths, but only one single wavelength at a time; thus, the light is divided into a spectrum from the very beginning without the need of a spectrometer [34]. Each laser frequency labels a different time delay, which is detected by interference and whenever the wavelength of the laser is swept, a single photodetector records the interference spectrum of the light waves returning to the device. The A-scan rate is determined by the frequency at which the light source is swept. Although the light source is more complex in the SS-OCT setting, compared to SD-OCT, the mechanism of the device is simplified, which contributes to data acquisition rates that are twice as fast [33]. The modulation of the reference arm length in the TD-OCT setting limits the speed of the scan, so the primary advantage of SD-OCT is its much higher acquisition speed. With its reference mirror remaining stationary, SD-OCT attains data quickly and renders images 40–110 times faster than TD-OCT devices. While the scan speed in TD-OCT is approximately 400 A-scans/s, it varies between 16,000 and 55,000 A-scans/s in SD-OCT, which means that a B-scan containing 2048 A-scans can be acquired in 0.04–0.13 s. This allows for three-dimensional

data sets to be achieved, which consists of a series of rapidly acquired B-scans. In the swept-source version of SD-OCT, up to a million A-scans can be obtained per second [30, 32].

Apart from highly increased scanning speeds, the fact that SS-OCT detects one single wavelength at a time avoids signal roll off, which occurs at the fringes of the imaging spectrum in FD-OCT, as the whole spectrum of wavelengths is detected at the same time. This results in enhanced depth range and enables for simultaneous imaging of different ocular structures without changing the focus of the device [30].

The overall resolution of the OCT image is determined by both axial and transverse resolution. As described above, transverse resolution depends on the beam diameter, while axial resolution depends on the properties of the optical light source. High spectral bandwidth leads to a short coherence length and high axial resolution [30, 32].

In TD-OCT, however, increasing the spectral bandwidth of the light source also involves higher electronic detection bandwidth, which results in a poor SNR. To overcome this problem, either the A-scan rate or depth scan range has to be decreased, or the incident optical power has to be increased, which is limited by the maximum permissible incident power on the eye, as stated by the American National Standards Institute (ANSI).

Both spectrometer- and swept-source-based SD-OCT systems benefit from higher speed and scan depth, enabling the acquisition of higher numbers of depth scans and resulting in high transverse resolution, which is not possible to achieve to the same extent in TD-OCT systems.

This sensitivity advantage over TD-OCT and the much shorter illumination time required allows for high-resolution imaging with illumination intensities well below the legal requirements [30, 32].

Another feature of SS-OCT is its capability of heterodyne detection, which means that the interferometric signal frequency spectrum is shifted away from the zero frequency. Hence, positive as well as negative displacements are taken into account [30].

The depth of tissue penetration depends on the wavelength of the light source. While SD-OCT usually employs an SLD with a wavelength of 800–900 nm, SS-OCT devices use wavelengths above 1000 nm. Shorter wavelengths involve higher degrees of scattering and attenuation, particularly from the retinal pigment epithelium (RPE), as it contains melanin. Consequently, SS-OCT is superior to SD-OCT in tissue penetration when it comes to increased tissue depth, dense retinal hemorrhage, exudates and imaging of structures beyond the RPE, such as the choroid or sclera. In SD-OCT, enhanced depth imaging (EDI), an averaging technique, has been employed to overcome this problem.

However, the longer wavelengths used in SS-OCTs result in a lower image resolution [30, 33–35].

## OCT and Dense Cataracts

As described in previous sections of this chapter, the introduction of PCI has significantly improved the accuracy of AL measurement, due to its higher precision compared to applanation ultrasound as well as its excellent intra- and interobserver reliability. The most important drawback of conventional PCI technology in contrast to ultrasound is its failure of measurement when it comes to dense posterior subcapsular (PSC), mature or brunescent cataracts, owing to a reduced SNR (<2.0) [36, 37]. Freeman et al. assessed cataract gradings (LOCS III) related to unsuccessful measurements using the IOL Master 500 and reported that AL values could not be obtained in either of the eyes with mature cataract. Additionally, they provided a clinical cut-off value for PSC cataracts (P-scale) of 3.5, as 100% of PSC cataracts exceeding a P-scale value of 3.5 failed to be measured using the PCI method. As the LOCS III grading system doesn't specify the location of the opacity, measurement failure may sometimes occur at lower levels (P-scale value >2.5). No significant relation could be detected for nuclear opalescence (NO) or cortical (C) cataracts. As visual acuity (VA) decreases with the development of

cataract, one could suggest VA to be related to measurement failure rates. While most of the data supports this conclusion, some patients with severe PSC cataracts can still retain good VA. Hence, the relationship is not strong enough to define a convenient cut-off value that defines whether IOL Master measurements will be obtainable [38].

The overall rate of acquisition failure for conventional PCI technology varies from 8% to 20% [36, 39–41], and could be reduced to 4.7% owing to the introduction of the composite scan method [25].

A newer approach to be used in optical biometry is SS-OCT, as employed in the IOL Master 700. The detailed differences between PCI and SS-OCT have been described in previous sections, but in general, the two technologies differ in terms of measurement setup and wavelength used (PCI: 780 nm; SS-OCT: 1055 nm) [37, 38].

Hirnschall et al. conducted a study to assess whether cases of measurement failure using the PCI method could be resolved by the SS-OCT technology. 1226 scans were evaluated, and measurement failure was defined as an SNR <2.0 in the IOL Master 500 acquisition. As the IOL Master 700 does not provide an SNR or a composite scan, each scan was analyzed separately and classified as successful if an AL value could be obtained and no warning was given by the device. Figure 10.6 shows a comparison of a successful and an unsuccessful SS-OCT scan. Twenty-one out of 23 (91.3%) of the unsuccessful scans using the PCI method were measurable with SS-OCT, yielding an estimated failure rate of 0.5%, when considering the total amount of participants (6/1226). Thus, SS-OCT was shown to significantly improve the rate of attainable AL measurements. While AL values of 80% of dense nuclear or white cataracts that failed to be measured by the IOL Master 500 could be attained by the IOL Master 700, all eyes with PSC cataract were measurable by the latter [37]. Similar results were reported by Srivannaboon et al. [42] and Akman et al. [43]

The main cause for the better outcomes of SS-OCT is that it operates with higher wavelengths compared to PCI. As higher wavelengths undergo lower amounts of light scattering, they result in a deeper penetration of tissue. The phenomenon which describes the correlation between wavelength and scattering is called Rayleigh scattering. It states that the amount of scattering is inversely proportional to the fourth power of the wavelength; thus, longer wavelengths are significantly less affected by Rayleigh scattering. Perhaps, the number of successful measurements could be further increased by using an even higher wavelength; however, it would happen at the cost of the scan resolution [37].

In general, the technology of SS-OCT significantly increases the number of successful AL measurements, but as in rare cases the scan acquisition is not feasible, optical biometry still cannot fully supersede ultrasonic biometry. In order to benefit from the higher accuracy of optical biometry, both techniques should be available in the presurgical setting, with ultrasound biometry being reserved for cases of measurement failure [38].

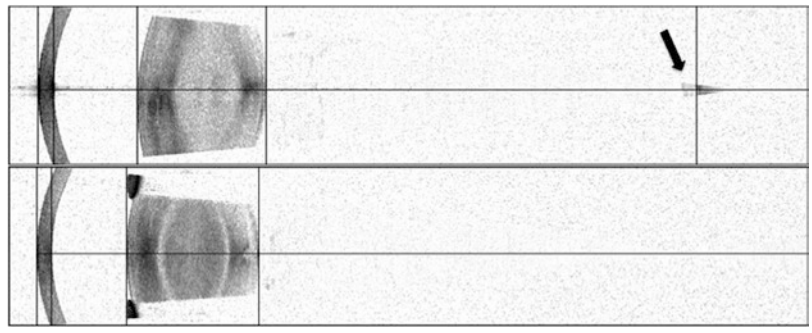

**Fig. 10.6** Comparison of a successful and an unsuccessful SS-OCT scan. The scan on top has successfully recognized the macula, while the scan at the bottom failed [37]

## Optical Biometry: Cornea

Besides accurate determination of ocular distances, such as AL or ACD, measurement of the corneal power is also critical for precise IOL power calculation [44].

Keratometry readings can be achieved using keratometers and topography devices. In manual keratometry, the measurement is limited to the central 3.0 mm of the anterior cornea. The curvature is determined at two axes; the first meridian measured is the steep meridian where the radius of curvature is smallest. This meridian yields the maximum keratometry reading (Max K). The second meridian determined is the axis that is 90° apart from the steep meridian, which equals the flat meridian with the minimum keratometry reading (Min K). Thus, besides the assessment of the corneal radius of curvature, the presence of corneal astigmatism as well as its degree and orientation can be determined [45].

One of the first devices developed for this purpose was the Javal-Schiøtz keratometer, a manual keratometer which utilizes the principals of reflection as well as fixed image size and variable object size. Its rotating mechanism enables measurements in multiple meridians. The cornea and tear film act as a reflecting surface in the shape of a convex mirror. The image of an object of known size and distance is reflected and analyzed to determine the curvature of the cornea over a 3.0–4.0 mm diameter area, depending on the dioptric power of the cornea [44–46]. As a result, the device generates the anterior corneal radius of curvature in millimeters [47]. To estimate the total corneal power, a theoretical calculation based on the anterior corneal curvature and a standard refractive index is applied [48]. Although the actual refractive index of the cornea is 1.376, a slightly lower index of 1.3375 is used to account for the shorter radius of curvature of the posterior corneal surface [49]. The measurement is performed at two paraxial corneal radii, and the assumption is made that the shape of the cornea between these two points is spherical. Hence, due to the aspheric corneal surface because of the flattening toward its periphery, measurements obtained by manual keratometry are only accurate for the central, spherical part of the cornea and moreover, those devices are of limited value in cases of irregularly shaped corneas [45, 49].

With developments in electronic systems, automated keratometers, which mostly use television monitors instead of an eyepiece system to view the reflected image, were introduced. A popular device is the Topcon automated keratorefractometer (Topcon, Tokyo, Japan), which simultaneously determines refraction and keratometry. For the purpose of keratometry, infrared light is used to illuminate the target mires and an infrared photodetector measures the image size to translate to radius of curvature [45, 49].

Although the Javal-Schiøtz keratometer and similar devices developed over time obtained useful measurements of regular spherocylindrical corneas, they were mainly replaced by optical biometry devices which simultaneously offer integrated keratometry measurement [47]. As refractive indices used in different devices may vary, it is more accurate to describe the cornea in terms of radius of curvature than power [49].

The IOL Master, as described above, relies on PCI for the measurement of AL, while an integrated automated keratometer similarly performs telecentric keratometry by implementing five measurements at six spots on a 2.5 mm diameter to obtain the average keratometry values at the two major perpendicular meridians [45]. Another optical biometry device to offer integrated keratometry is the Lenstar LS900. While the device differs from the IOL Master in measuring optical distances, as it uses OLCR instead of PCI, the same technology is used to measure keratometry readings [50].

Many of the subsequently introduced devices are based on the Placido disk principle. The patient fixates at the center of a disc painted with alternating black and white rings, which are reflected from the anterior cornea and the reflections are analyzed to gain information about the surface shape of the cornea and to calculate its radius of curvature. A schematic diagram of a Placido disk topographer is shown in Fig. 10.7.

While keratoscopy using a Placido disk was initially complicated and time-consuming, as a

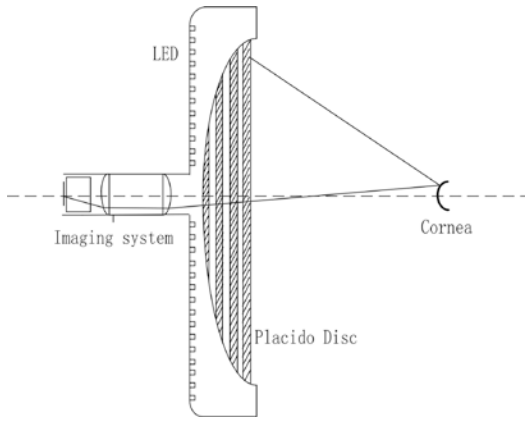


**Fig. 10.7** Schematic diagram of a Placido disk topographer [51]

handheld device was used, following photography of the reflections and comparison of the photographs to images reflected by spheres of known radius, computer technology enabled the development of an automated use of the Placido disk. Many modern devices, such as some videokeratography devices, rely on the Placido disk principle. In computer-assisted videokeratography, computer programs are used to derive topographic information from a high-resolution cylindrical photokeratoscope. The images are digitized and, at the same time, displayed as color-coded maps of corneal power, photokeratoscopic images, wire mesh models, or solid models. Examples of commercially available systems are the EyeSys 3000 (EyeSys Laboratories, Houston, USA) and the TMS-I (Computer Anatomy Inc., New York, USA). A disadvantage of those devices is that they only take into account the anterior corneal surface and various assumptions must still be made regarding the relationship between the anterior and posterior corneal surface, in order to calculate the total corneal power [46, 49].

The primary advantage of modern technologies, which include slit-scanning Scheimpflug photography, very high-frequency ultrasound and optical coherence tomography, are increased accuracy, an extended area of measurement and the ability to directly measure the posterior corneal surface [46]. Those devices offer simulated keratometry readings (Sim K), based on the central 3.0 mm of the anterior corneal curvature alone, to allow for comparison with other instruments [44].

The first device to offer the possibility of measuring the posterior corneal surface was the Orbscan (Orbtek Inc., New York, USA), which uses optical slit-scanning. The cornea is scanned by multiple slit light beams to obtain two-dimensional, cross-sectional images which are then translated to a topographical map. The newer Orbscan II (Bausch & Lomb, New York, USA) and the TMS 5 (Tomey GmbH, Nürnberg, Germany) combine the slit-scanning method with a Placido disk to take advantage of both technologies [46]. Ring topography and slit-scan images are taken separately, and after the assessment of both, the data is merged [50].

Another keratometric method is Scheimpflug photography, whose technique is employed in the Pentacam (Oculus Inc., Wetzlar, Germany), the GALILEI (Zeimer Group, Port, Switzerland), and the SIRIUS (CSO, Scandicci, Italy). The Scheimpflug principle describes a condition that allows documentation of an obliquely tilted object (i.e., the planes of image, lens, and object are not parallel to each other) with maximum depth of focus and minimum image distortion. The principle allows for a specific arrangement of the three planes in order to increase the focal depth. In Scheimpflug photography, a rotating camera captures images of the anterior eye segment at different meridians around the optical axis, including anterior corneal surface, posterior corneal surface, and lens. In approximately 2 s, between 25 and 50 slit images are taken, with 500 elevation points incorporated in every one of them. A three-dimensional model of the anterior eye segment is created, and the software incorporated in the device calculates and displays topographical maps as well as power maps of the cornea (Fig. 10.8) [46, 50, 52].

Another method for corneal imaging is very high-frequency ultrasound. This technique is used in the Artemis (ArcScan Inc., Golden, USA) to allow for a direct visualization and measurement of the posterior corneal surface. Furthermore, three-dimensional maps of individual corneal layers can be obtained, which makes

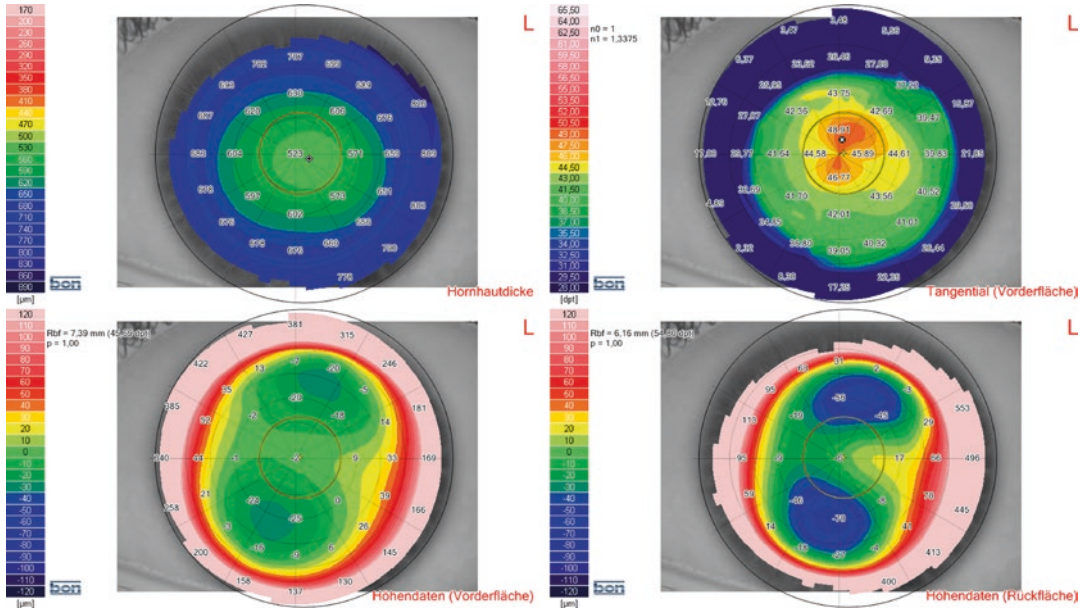


**Fig. 10.8** Topographical maps and power maps of the cornea, generated by Scheimpflug photography

it an important tool in the field of keratorefractive surgery [46].

SS-OCT devices, such as the Casia 2 (Tomey, Nagoya, Japan), which is designed specifically for imaging the anterior segment, can be used for keratometric purposes. It is indicated for cross-sectional imaging of the anterior segment components such as anterior chamber or cornea, as well as for their dimension measurements such as curvature, length, area, or volume. To generate corneal maps, the shape of the cornea is analyzed similar to a topographer [53].

For all those devices, attention has to be paid to patients who underwent keratorefractive surgery prior to the measurement procedure, as their K readings need correction concerning the refractive power of the cornea and the predicted postoperative IOL position [47].

Although all these techniques provide reasonable results to be used in IOL power calculation, discrepancies concerning the mean spherical equivalent were found when comparing the devices. Those discrepancies may arise due to differences in the optical or mathematical methods used to calculate the total corneal power. Hamer et al. compared the results of different keratometers and found the corneal curvature to be measured steepest with the manual keratometer, followed by automated keratometry and Scheimpflug imaging. The flattest measurements were obtained with instruments that calculated Sim K from Placido disc topography. The corneal curvature was steeper when measured with the IOL Master compared to Placido disc topographers, which can be attributed to the small area that is used to simulate the K readings [44]. Reuland et al. compared the IOL Master and the Pentacam and showed that the results of the two devices are comparable [54].

The assessment of the mean spherical equivalent does not depend on the orientation of the power meridians and is therefore affected to a lower extent by erroneous readings at one meridian than the determination of astigmatic orientation and power. The latter is more prone to variable outcomes, which can be evaluated by intra-observer, interobserver, and between-session repeatability. In the study conducted by Hamer et al., repeatability was weaker for topographic devices and manual keratometers when compared to the Pentacam and the IOL Master.

The tear film has a significant influence on the repeatability of corneal topographers due to the likelihood of localized disturbances in an unsta-

ble tear film that may affect readings along a specific meridian and hence distort the measurement of astigmatism. This limitation, from which devices based on the Placido principle suffer more than those based on Scheimpflug imaging or automated keratometry, can be counteracted by administrating ocular lubricants prior to the measurement in order to stabilize the tear film [44]. However, instruments working with Placido discs deliver a higher level of spatial resolution compared to Scheimpflug devices and SS-OCT [50]. Instruments such as the IOL Master are more resistant to tear film-induced errors, owing to the small measurement zone. Furthermore, the integrated software provides numerous quality checks that may improve the measurement's reliability [44].

Concerning the Pentacam, total corneal power, which includes both the anterior and posterior corneal curvature, is a better representative for subjective cylinder than Sim K.

Devices that combine two methods, such as hybrid topographers, in which the anterior corneal surface is measured by the Placido disk principle, while Scheimpflug imaging is used for both the anterior and posterior surface, can potentially achieve more accurate results than one of the two techniques alone. Therefore, the results obtained by the TMS 5 are superior to Placido or Scheimpflug measurements alone [50]. Keratometric data can also be merged with topographic output to improve the results [55].

Hoffmann et al. compared multiple keratometry devices to the newer anterior segment OCT Casia SS-1000 and reported that SS-OCT measurements offer not only a good reproducibility in normal eyes but also in post-LASIK eyes and eyes with keratoconus. In their series, Casia SS-1000 delivered the best predictive power concerning astigmatism, compared to the Lenstar LS900 and the Pentacam. This may be due to the fact that it renders images much faster than the Pentacam and therefore minimizes motion artefacts. The results of the TMS 5 were comparable to the Casia SS-1000 [50].

In general, when calculating toric IOLs, not only the anterior but also the posterior corneal surface should be taken into account, as it plays a significant role when evaluating the total amount of corneal astigmatism. While keratometric data is more stable than tomographic data, corneal tomography is more precise, as it includes the measurement of the posterior corneal curvature. For most patients, the best results may be obtained by combined keratometry, topography of the anterior corneal curvature, and tomography of the anterior and posterior curvature. Anterior segment OCT may be a useful tool for corneal tomography [5].

## Intraoperative OCT

As discussed in previous sections of this chapter, modern techniques such as optical biometry have significantly improved IOL power calculation during the last decades. Although the latest generation of IOL power calculation formulae has further enhanced the postoperative refractive outcome, a relevant unpredictability still remains. When aiming for emmetropia, approximately 8.5% of all patients need a refractive correction of more than 1.0 D after cataract surgery, as stated by the data collected by the EUREQUO system for the purpose of quality control [56]. The incidence of unsatisfactory refractive outcomes depends on the length of the eye and is particularly apparent in shorter eyes (~30%) [57]. As shown by Olsen [6] and Norrby [58], the main source of postoperative refractive errors is an imprecise prediction of the final postoperative IOL position or postoperative ACD. In modern IOL power formulae, the so-called effective lens position (ELP), which is a virtual position predicted by preoperative measurements such as corneal radii, AL, or ACD, was developed to optimize the formulae for empirical data [59, 60]. However, the ELP does not directly correlate with the anatomical IOL position and is not capable of predicting the IOL position after surgery or the ACD shift within the first postoperative months with certainty [59]. It was shown that a better prediction factor for the final postoperative IOL position, compared to preoperative methods, is the real-time assessment of the intraoperative distance between the endothelium and the anterior lens capsule of the aphakic eye [57, 61].

The field of intraoperative OCT (iOCT) has advanced in several ways in recent years. The first iOCT system, which was a handheld probe that employed time-domain detection, was reported in 2001 by Radhakrishnan [62]. With the advent of Fourier-domain techniques, iOCT systems have further developed, using both spectrometer and swept-source systems to increase measurement speed and to allow for larger field-of-views and higher sampling densities [63]. Handheld probes had the advantage that the patient's head did not need to be positioned at a chin-rest, thus allowing image acquisition in supine position as well as in sterile settings for the first time, which was the major shift that initiated the evolution of OCT into the operating room. However, the images were affected by motion artefacts, they had a challenging reproducibility and frequent pauses were required during surgery for image acquisition. To address these issues, in a first attempt, the devices were mounted on conventional operating microscopes and later permanently integrated into the microscope optics to combine the two optical paths, allowing for visualization of two-dimensional OCT sections through the microscope's oculars or on an external display, thus providing the opportunity of real-time OCT during surgery [64]. Current-generation microscope-integrated iOCT systems can be combined either with direct or with indirect ophthalmic viewing systems and enable both anterior and posterior segment imaging intraoperatively [63].

In cataract surgery, microscope-integrated OCT is used extensively in training novel surgeons to improve surgical precision [64, 65]. It can be used to visualize corneal incisions, to evaluate the adequacy of stroma hydration at the end of the procedure to prevent postoperative wound leak or to assess trenching depth during phacoemulsification in order to prevent iatrogenic capsular rupture. Senior surgeons may also benefit from microscope-integrated OCT when facing clinically suspected complicated cases, such as identifying a true posterior polar cataract or capsular defects in traumatic cataracts [64].

In patients with mature cataracts in whom preoperative AL acquisition failed, iOCT can be used to assess AL values prior to IOL implantation. Moreover, it can be helpful in patients with very low compliance.

The idea behind using iOCT for biometrical purposes, particularly for ACD measurement, stems from the lens haptic plane concept. The lens haptic plane can be considered the plane through the vertices of the IOL haptics, which is associated with the anatomical position of the IOL to be implanted, hence its fixation plane, when the site of fixation equals the equator of the capsular bag. The lens haptic plane is reasonably independent of the IOL model used [66, 67]. Measuring the anterior lens capsule of the aphakic eye intraoperatively allows to depict a position close to the theoretical lens haptic plane [57].

To evaluate the benefit of iOCT for ocular biometry, Hirnschall et al. performed intraoperative ACD measurements to predict the postoperative IOL position. They used a prototype of a continuous iOCT that was directly connected to the surgical microscope. In the surgical setting, intraoperative measurements of the aphakic eye were obtained following phacoemulsification and implantation of a capsular tension ring to tauten the lens capsule. A partial least-square regression model for ACD was created that proved the distance between corneal endothelium and anterior lens capsule to be a significantly better predictor for postoperative ACD compared to preoperative measurements. Intraoperatively measured ACD had the highest predictive power, and AL had the second highest predictive power, followed by preoperatively measured ACD. Improvement could further be achieved by using regression models combining preoperative and intraoperative ACD measurements [57, 59].

In the second step, Hirnschall et al. evaluated whether the implication of intraoperatively measured ACD into IOL power calculation formulae improves the postoperative refractive outcome. A partial least-regression model was generated to compare conventional optimized formulae with a formula including the ACD measured intraoperatively. As a result, it was shown that the latter was useful to better predict postoperative refraction and AL dependency could be significantly lowered. Future steps may be an automation of iOCT

as well as its implementation into fourth-generation power formulae or ray tracing using the anatomical lens position instead of the currently used virtual ELP [60].

Optical biometry has evolved significantly in the last decades. Accuracy in preoperative measurements is vital for satisfactory postoperative refractive outcomes, so the latest biometry technologies combined with newer IOL power calculation formulae and lens designs have become necessary tools in the field of cataract surgery. With all the developments discussed in the chapter, refractive outcomes in a range of ±0.5 D have become achievable in a majority of the patients. However, as the attainment of the target postoperative refraction is not achieved in all cases, further research is still required [68].

## References


1. Drexler W, Findl O, Menapace R, Rainer G, Vass C, Hitzenberger CK, Fercher AF. Partial coherence interferometry: a novel approach to biometry in cataract surgery. Am J Ophthalmol. 1998;126(4):524–34. https://doi.org/10.1016/S0002-9394(98)00113-5.
2. Fontes BM, Fontes BM, Castro E. Intraocular lens power calculation by measuring axial length with partial optical coherence and ultrasonic biometry. Arq Bras Oftalmol. 2011;74(3):166–70. https://doi.org/10.1590/S0004-27492011000300004.
3. Goto S, Maeda N, Noda T, Ohnuma K, Koh S, Iehisa I, Nishida K. Comparison of composite and segmental methods for acquiring optical axial length with swept-source optical coherence tomography. Sci Rep. 2020;10(1):4474. https://doi.org/10.1038/s41598-020-61391-7.
4. Hitzenberger CK, Fercher AF, Juchem M. Measurement of the axial eye length and retinal thickness by laser Doppler interferometry. In: Puliafito CA, editor. Optics, electro-optics, and laser applications in science and engineering. SPIE; 1991. p. 46–50. https://doi.org/10.1117/12.43956.
5. Lee AC, Qazi MA, Pepose JS. Biometry and intraocular lens power calculation. Curr Opin Ophthalmol. 2008;19(1):13–7. https://doi.org/10.1097/ICU.0b013e3282f1c5ad.
6. Olsen T. Sources of error in intraocular lens power calculation. J Cataract Refract Surg. 1992;18(2):125–9. https://doi.org/10.1016/S0886-3350(13)80917-0.
7. Ivanov AP, Chaikovskii AP, Kumeisha AA. New method for high-range resolution measurements of light scattering in optically dense inhomogeneous media. Opt Lett. 1977;1(6):226. https://doi.org/10.1364/OL.1.000226.
8. Hitzenberger CK, Drexler W, Leitgeb RA, Findl O, Fercher AF. Key developments for partial coherence biometry and optical coherence tomography in the human eye made in Vienna. Invest Opthalmol Vis Sci. 2016;57(9):OCT460. https://doi.org/10.1167/iovs.16-19362.
9. Fercher AF, Roth E. Ophthalmic laser interferometry. In: Mueller GJ, editor. Optical instrumentation for biomedical laser applications, vol. 658. SPIE; 1986. p. 48. https://doi.org/10.1117/12.938523.
10. Hitzenberger CK. Optical measurement of the axial eye length by laser Doppler interferometry. Invest Ophthalmol Vis Sci. 1991;32(3):616–24.
11. Kunert KS, Peter M, Blum M, Haigis W, Sekundo W, Schütze J, Büehren T. Repeatability and agreement in optical biometry of a new swept-source optical coherence tomography–based biometer versus partial coherence interferometry and optical low-coherence reflectometry. J Cataract Refract Surg. 2016;42(1):76–83. https://doi.org/10.1016/j.jcrs.2015.07.039.
12. Findl O, Drexler W, Menapace R, Heinzl H, Hitzenberger CK, Fercher AF. Improved prediction of intraocular lens power using partial coherence interferometry. J Cataract Refract Surg. 2001;27(6):861–7. https://doi.org/10.1016/S0886-3350(00)00699-4.
13. Cech R, Utíkal T, Juhászová J. [Comparison of optical and ultrasound biometry and assessment of using both methods in practice]. Ceska Slov Oftalmol Cas Ceske Oftalmol Spolecnosti Slov Oftalmol Spolecnosti. 2014;70(1):3–9.
14. Drexler W. Measurement of the thickness of fundus layers by partial coherence tomography. Opt Eng. 1995;34(3):701. https://doi.org/10.1117/12.191809.
15. Cantor LB, Rapuano CJ, Cioffi GA. Basic and clinical science course (BCSC), section 03: clinical optics. American Academy of Ophthalmology; 2014.
16. Hitzenberger C, Mengedoht K, Fercher AF. [Laser optic measurements of the axial length of the eye]. Fortschritte Ophthalmol Z Dtsch Ophthalmol Ges. 1989;86(2):159–61.
17. Kohnen T, editor. Modern cataract surgery. Karger; 2002.
18. Sacu S, Findl O, Buehl W, Kiss B, Gleiss A, Drexler W. Optical biometry of the anterior eye segment: interexaminer and intraexaminer reliability of ACMaster. J Cataract Refract Surg. 2005;31(12):2334–9. https://doi.org/10.1016/j.jcrs.2005.04.035.
19. Lavanya R, Teo L, Friedman DS, Aung HT, Baskaran M, Gao H, Alfred T, Seah SK, Kashiwagi K, Foster PJ, Aung T. Comparison of anterior chamber depth measurements using the IOLMaster, scanning peripheral anterior chamber depth analyser, and anterior segment optical coherence tomography. Br J Ophthalmol. 2007;91(8):1023–6. https://doi.org/10.1136/bjo.2006.113761.
20. Buehl W, Stojanac D, Sacu S, Drexler W, Findl O. Comparison of three methods of measuring corneal thickness and anterior chamber depth. Am J Ophthalmol. 2006;141(1):7–12.e1. https://doi.org/10.1016/j.ajo.2005.08.048.

21. Kriechbaum K, Leydolt C, Findl O, Bolz M, Drexler W. Comparison of partial coherence interferometers: Acmaster versus laboratory prototype. J Refract Surg (Thorofare, NJ, 1995). 2006;22(8):811–6.
22. Huang J, McAlinden C, Huang Y, Wen D, Savini G, Tu R, Wang Q. Meta-analysis of optical low-coherence reflectometry versus partial coherence interferometry biometry. Sci Rep. 2017;7(1):43414. https://doi.org/10.1038/srep43414.
23. Hoffer KJ, Shammas JH, Savini G. Comparison of 2 laser instruments for measuring axial length. J Cataract Refract Surg. 2010;36(4):644–8. https://doi.org/10.1016/j.jcrs.2009.11.007.
24. Epitropoulos A. Axial length measurement acquisition rates of two optical biometers in cataractous eyes. Clin Ophthalmol. 2014;8:1369. Published online Jul 2014. https://doi.org/10.2147/OPTH.S62653.
25. Hirnschall N, Murphy S, Pimenides D, Maurino V, Findl O. Assessment of a new averaging algorithm to increase the sensitivity of axial eye length measurement with optical biometry in eyes with dense cataract. J Cataract Refract Surg. 2011;37(1):45–9. https://doi.org/10.1016/j.jcrs.2010.07.023.
26. Dietlein TS, Roessler G, Lüke C, Dinslage S, Roters S, Jacobi PC, Walter P, Krieglstein GK. Signal quality of biometry in silicone oil–filled eyes using partial coherence laser interferometry. J Cataract Refract Surg. 2005;31(5):1006–10. https://doi.org/10.1016/j.jcrs.2004.09.049.
27. Suto C, Sato C, Shimamura E, Toshida H, Ichikawa K, Hori S. Influence of the signal-to-noise ratio on the accuracy of IOLMaster measurements. J Cataract Refract Surg. 2007;33(12):2062–6. https://doi.org/10.1016/j.jcrs.2007.07.031.
28. Szkulmowski M, Wojtkowski M. Averaging techniques for OCT imaging. Opt Express. 2013;21(8):9757. https://doi.org/10.1364/OE.21.009757.
29. Huang D, Swanson E, Lin C, Schuman J, Stinson W, Chang W, Hee M, Flotte T, Gregory K, Puliafito C, et al. Optical coherence tomography. Science. 1991;254(5035):1178–81. https://doi.org/10.1126/science.1957169.
30. Yaqoob Z, Wu J, Yang C. Spectral domain optical coherence tomography: a better OCT imaging strategy. BioTechniques. 2005;39(6S):S6–S13. https://doi.org/10.2144/000112090.
31. Drexler W, Fujimoto JG, editors. Optical coherence tomography. Springer International Publishing; 2015. https://doi.org/10.1007/978-3-319-06419-2.
32. Schuman JS. Spectral domain optical coherence tomography for glaucoma (an AOS thesis). Trans Am Ophthalmol Soc. 2008;106:426–58.
33. Alibhai YA, Or C, Witkin AJ. Swept source optical coherence tomography: a review. Curr Ophthalmol Rep. 2018;6(1):7–16. https://doi.org/10.1007/s40135-018-0158-3.
34. Kishi S. Impact of swept source optical coherence tomography on ophthalmology. Taiwan J Ophthalmol. 2016;6(2):58–68. https://doi.org/10.1016/j.tjo.2015.09.002.
35. Cole ED, Duker JS. OCT technology: will we be "swept" away? Rev Ophthalmol. Published online Apr 2017. https://www.reviewofophthalmology.com/article/oct-technology-will-we-be-swept-away.
36. Kiss B, Findl O, Menapace R, Wirtitsch M, Drexler W, Hitzenberger CK, Fercher AF. Biometry of cataractous eyes using partial coherence interferometry: clinical feasibility study of a commercial prototype I. J Cataract Refract Surg. 2002;28(2):224–9. https://doi.org/10.1016/s0886-3350(01)01272-x.
37. Hirnschall N, Varsits R, Doeller B, Findl O. Enhanced penetration for axial length measurement of eyes with dense cataracts using swept source optical coherence tomography: a consecutive observational study. Ophthalmol Ther. 2018;7(1):119–24. https://doi.org/10.1007/s40123-018-0122-1.
38. Freeman G, Pesudovs K. The impact of cataract severity on measurement acquisition with the IOLMaster. Acta Ophthalmol Scand. 2005;83(4):439–42. https://doi.org/10.1111/j.1600-0420.2005.00473.x.
39. Rajan MS, Keilhorn I, Bell JA. Partial coherence laser interferometry vs conventional ultrasound biometry in intraocular lens power calculations. Eye. 2002;16(5):552–6. https://doi.org/10.1038/sj.eye.6700157.
40. Findl O, Drexler W, Menapace R, Hitzenberger CK, Fercher AF. High precision biometry of pseudophakic eyes using partial coherence interferometry. J Cataract Refract Surg. 1998;24(8):1087–93. https://doi.org/10.1016/S0886-3350(98)80102-8.
41. Haigis W, Lege B, Miller N, Schneider B. Comparison of immersion ultrasound biometry and partial coherence interferometry for intraocular lens calculation according to Haigis. Graefes Arch Clin Exp Ophthalmol. 2000;238(9):765–73. https://doi.org/10.1007/s004170000188.
42. Srivannaboon S, Chirapapaisan C, Chonpimai P, Loket S. Clinical comparison of a new swept-source optical coherence tomography–based optical biometer and a time-domain optical coherence tomography–based optical biometer. J Cataract Refract Surg. 2015;41(10):2224–32. https://doi.org/10.1016/j.jcrs.2015.03.019.
43. Akman A, Asena L, Güngör SG. Evaluation and comparison of the new swept source OCT-based IOLMaster 700 with the IOLMaster 500. Br J Ophthalmol. 2016;100(9):1201–5. https://doi.org/10.1136/bjophthalmol-2015-307779.
44. Hamer CA, Buckhurst H, Purslow C, Shum GL, Habib NE, Buckhurst PJ. Comparison of reliability and repeatability of corneal curvature assessment with six keratometers: comparison of six keratometers. Clin Exp Optom. 2016;99(6):583–9. https://doi.org/10.1111/cxo.12329.
45. Mehravaran S, Asgari S, Bigdeli S, Shahnazi A, Hashemi H. Keratometry with five different techniques: a study of device repeatability and inter-device agreement. Int Ophthalmol. 2014;34(4):869–75. https://doi.org/10.1007/s10792-013-9895-3.
46. Gutmark R, Guyton DL. Origins of the keratometer and its evolving role in ophthalmology. Surv

Ophthalmol. 2010;55(5):481–97. https://doi.org/10.1016/j.survophthal.2010.03.001.
47. Hirnschall N, Findl O. Patient-assessment techniques for cataract surgery. Expert Rev Ophthalmol. 2011;6(2):211–9. https://doi.org/10.1586/eop.11.4.
48. Hoshikawa R, Kamiya K, Fujimura F, Shoji N. Comparison of conventional keratometry and total keratometry in normal eyes. Biomed Res Int. 2020;2020:1–6. https://doi.org/10.1155/2020/8075924.
49. Fowler CW, Dave TN. Review of past and present techniques of measuring corneal topography. Ophthalmic Physiol Opt. 1994;14(1):49–58. https://doi.org/10.1111/j.1475-1313.1994.tb00556.x.
50. Hoffmann PC, Abraham M, Hirnschall N, Findl O. Prediction of residual astigmatism after cataract surgery using swept source Fourier domain optical coherence tomography. Curr Eye Res. 2014;39(12):1178–86. https://doi.org/10.3109/02713683.2014.898376.
51. Sui C, Wo S, Cai P, Gao N, Xu D, Han Y, Du C. Design and implementation of optical system for Placido-disc topography. J Mod Opt. 2017;64(21):2413–9. https://doi.org/10.1080/09500340.2017.1366567.
52. Wegener A, Laser-Junga H. Photography of the anterior eye segment according to Scheimpflug's principle: options and limitations—a review. Clin Exp Ophthalmol. 2009;37(1):144–54. https://doi.org/10.1111/j.1442-9071.2009.02018.x.
53. Angmo D, Nongpiur M, Sharma R, Sidhu T, Sihota R, Dada T. Clinical utility of anterior segment swept-source optical coherence tomography in glaucoma. Oman J Ophthalmol. 2016;9(1):3. https://doi.org/10.4103/0974-620X.176093.
54. Reuland MS, Reuland AJ, Nishi Y, Auffarth GU. Corneal radii and anterior chamber depth measurements using the IOLmaster versus the Pentacam. J Refract Surg (Thorofare, NJ, 1995). 2007;23(4):368–73.
55. Hoffmann PC, Wahl J, Hütz WW, Preußner P-R. A ray tracing approach to calculate toric intraocular lenses. J Refract Surg. 2013;29(6):402–8. https://doi.org/10.3928/1081597X-20130515-04.
56. Lundström M, Barry P, Henry Y, Rosen P, Stenevi U. Evidence-based guidelines for cataract surgery: guidelines based on data in the European registry of quality outcomes for cataract and refractive surgery database. J Cataract Refract Surg. 2012;38(6):1086–93. https://doi.org/10.1016/j.jcrs.2012.03.006.
57. Hirnschall N, Farrokhi S, Amir-Asgari S, Hienert J, Findl O. Intraoperative optical coherence tomography measurements of aphakic eyes to predict postoperative position of 2 intraocular lens designs. J Cataract Refract Surg. 2018;44(11):1310–6. https://doi.org/10.1016/j.jcrs.2018.07.044.
58. Norrby S. Sources of error in intraocular lens power calculation. J Cataract Refract Surg. 2008;34(3):368–76. https://doi.org/10.1016/j.jcrs.2007.10.031.
59. Hirnschall N, Amir-Asgari S, Maedel S, Findl O. Predicting the postoperative intraocular lens position using continuous intraoperative optical coherence tomography measurements. Invest Opthalmol Vis Sci. 2013;54(8):5196. https://doi.org/10.1167/iovs.13-11991.
60. Hirnschall N, Norrby S, Weber M, Maedel S, Amir-Asgari S, Findl O. Using continuous intraoperative optical coherence tomography measurements of the aphakic eye for intraocular lens power calculation. Br J Ophthalmol. 2015;99(1):7–10. https://doi.org/10.1136/bjophthalmol-2013-304731.
61. Pujari A, Agarwal D, Chawla R, Kumar A, Sharma N. Intraoperative optical coherence tomography guided ocular surgeries: critical analysis of clinical role and future perspectives. Clin Ophthalmol. 2020;14:2427–40. https://doi.org/10.2147/OPTH.S270708.
62. Radhakrishnan S. Real-time optical coherence tomography of the anterior segment at 1310 nm. Arch Ophthalmol. 2001;119(8):1179. https://doi.org/10.1001/archopht.119.8.1179.
63. El-Haddad MT, Tao YK. Advances in intraoperative optical coherence tomography for surgical guidance. Curr Opin Biomed Eng. 2017;3:37–48. https://doi.org/10.1016/j.cobme.2017.09.007.
64. Posarelli C, Sartini F, Casini G, Passani A, Toro MD, Vella G, Figus M. What is the impact of intraoperative microscope-integrated OCT in ophthalmic surgery? Relevant applications and outcomes. A systematic review. J Clin Med. 2020;9(6):1682. https://doi.org/10.3390/jcm9061682.
65. Carrasco-Zevallos OM, Viehland C, Keller B, Draelos M, Kuo AN, Toth CA, Izatt JA. Review of intraoperative optical coherence tomography: technology and applications [Invited]. Biomed Opt Express. 2017;8(3):1607. https://doi.org/10.1364/BOE.8.001607.
66. Norrby SNE, Koranyi G. Prediction of intraocular lens power using the lens haptic plane concept. J Cataract Refract Surg. 1997;23(2):254–9. https://doi.org/10.1016/S0886-3350(97)80350-1.
67. Norrby NES. The lens haptic plane (LHP) a fixed reference for IOL implant power calculation. Eur J Implant Refract Surg. 1995;7(4):202–9. https://doi.org/10.1016/S0955-3681(13)80035-4.
68. Nazm N, Chakrabarti A. Update on optical biometry and intraocular lens power calculation. TNOA J Ophthal Sci Res. 2017;55(3):196. https://doi.org/10.4103/tjosr.tjosr_44_17.